ACS APPLIED MATERIALS & INTERFACES

Research Article

www.acsami.org

Ultrathin $BaTiO_3$ Nanowires with High Aspect Ratio: A Simple One-Step Hydrothermal Synthesis and Their Strong Microwave Absorption

Jin Yang,[†,§] Jie Zhang,[†,§] Chongyun Liang,[‡] Min Wang,[†] Pengfei Zhao,[†] Mengmei Liu,[†] Jiwei Liu,[†] and Renchao Che*,[†]

[†]Department of Materials Science and Advanced Materials Laboratory, and [‡]Department of Chemistry, Fudan University, Shanghai 200438, P. R. China

Supporting Information

ABSTRACT: In this paper, we report the facile synthesis of ultrathin barium titanate ($BaTiO_3$) nanowires with gram-level yield via a simple one-step hydrothermal treatment. Our $BaTiO_3$ nanowires have unique features: single crystalline, uniform size distribution and ultra high aspect ratio. The synergistic effects including both Ostwald ripening and cation exchange reaction are responsible for the growth of the ultrathin $BaTiO_3$ nanowires. The microwave absorption capability of the ultrathin $BaTiO_3$ nanowires is improved compared to that of $BaTiO_3$ nanotorus,[1] with a maximum reflection loss as high as −24.6 dB at 9.04 GHz and an absorption bandwidth of 2.4 GHz (<−10 dB). Our method has some novel advantages: simple, facile, low cost and high synthesis yield, which might be developed to prepare other ferroelectric nanostructures. The strong microwave absorption property of the ultrathin $BaTiO_3$ nanowires indicates that these nanowires could be used as promising materials for microwave-absorption and stealth camouflage techniques.

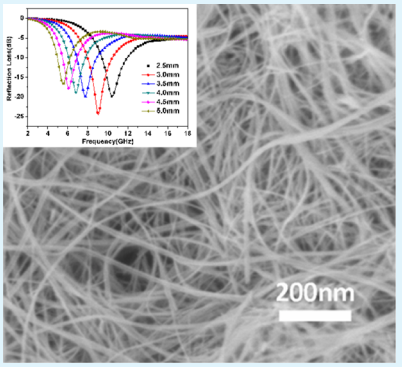

KEYWORDS: *$BaTiO_3$ nanowires, ultrathin, microwave absorption, transmission electron microscopy*

1. INTRODUCTION

Recently, electromagnetic (EM) interference and shielding have been becoming hot topics in the fields of camouflage defending and anticontamination of electromagnetic signal. Considerable attention has been paid to the development of innovative microwave absorbers. Size or geometrical morphology of one microwave absorber plays a key role in its microwave absorption properties.[2] One-dimensional (1D) nanostructures can be used for efficient absorber due to the dissipation effects for electrons and phonons scattered by the periodical boundary conditions within nanocrystals. $BaTiO_3$ has been attracting extensive attention as a result of their excellent dielectric properties, thus, in possession of applications in the fields of multilayer capacitors, thermistors, electro-optical devices, and electromechanical devices.[3,4] As ferroelectrics, $BaTiO_3$ typically undergo a marked relaxation in their dielectric properties, which in turn leads to a decrease in relative permittivity with frequency, accompanied by a resonance peak in the dielectric loss within a narrow frequency band. McNeal et al. have carefully investigated the dielectric properties of $BaTiO_3$ ceramics and particles at microwave frequencies as a function of grain/particle size and found the origin of the relaxation phenomenon has been attributed to the existence of domain structure.[5,6] Also it is evident that the microwave dielectric relaxation phenomena are dependent on particle size and morphology. $BaTiO_3$ and its composites[7] has been considered as a type of microwave absorber at gigahertz frequencies.[8,9]

So far, many different methods have been reported about the fabrication of 1D $BaTiO_3$ nanostructures. The major methods include hydrothermal reaction and molten-salt synthesis.[10] On the one hand, Park and co-workers synthesized single crystalline $BaTiO_3$ nanorods using bimetallic alkoxide as precursors under solution phase decomposition conditions.[11,12] By a template-free method, Joshi and co-workers synthesized single crystalline $BaTiO_3$ nanowires from TiO_2 as a starting material by a hydrothermal method. However, the unexpected large $BaTiO_3$ particles with irregular morphologies might occur.[13] Kang and co-workers fabricated single-crystalline $BaTiO_3$ nanowires using titanate nanorods as a precursor.[14,15] On the other hand, by a solid-state chemical reaction using NaCl as a type of molten salt, single crystalline $BaTiO_3$ nanowires and $SrTiO_3$ nanocubes were synthesized.[16] Hsish and co-workers reported a morphology-controlled synthesis of $BaTiO_3$ nanostructures with the help of NaCl-KCl flux at 700 °C.[17] Very recently, $BaTiO_3$ nanotubes with an average diameter of ∼10 nm were synthesized via a wet chemical route and its microwave absorption properties were studied.[18,19]

Received: April 23, 2013
Accepted: July 2, 2013
Published: July 2, 2013

Our group investigated the hydrothermal synthesis and microwave absorption properties of $BaTiO_3$ nanotorus. The microwave absorption of hollow $BaTiO_3$ nanotorus could be enhanced compared to that of the solid $BaTiO_3$ nanoparticles.[1]

Herein, based on Ostwald ripening and cation exchange mechanisms, we propose a facile one-step hydrothermal synthesis, using both aqueous and ethonal medium under alkaline conditions to produce ultrathin $BaTiO_3$ nanowires with ultra high aspect ratio (>1300) and gram-level yield. The morphology, microstructure and microwave absorption of the ultrathin $BaTiO_3$ nanowires were comprehensively characterized by X-ray diffraction (XRD), Raman spectrum, field-emission scanning electron microscopy (FESEM), field emission transmission electron microscopy (FETEM) and microwave absorption examination at 2−18 GHz. An enhanced microwave absorption property with a strong absorption peak of −24.6 dB at 9.04 GHz was found from the ultrathin $BaTiO_3$ nanowires compared to that of the conventional $BaTiO_3$ nanotorus and nanoparticles. As far as we know, $BaTiO_3$ nanowires with diameter less than 10 nm, aspect ratio more than 1300 and yield with gram-level have never been reported previously. Our novel synthesis method has many advantages: simple, low-cost, high productivity, high purity, and perfect uniformity of the products. Moreover, all the raw materials are commercially accessible and the cost of the experimental equipments is quite cheap. Because of the simplicity of this method, it is anticipated that this methodology can be expanded to the large-scale synthesis of other important ferroelectric nanostructures.

2. EXPERIMENTAL SECTION

2.1. Materials. Potassium hydroxide (KOH), polyethylene glycol (PEG 6000), tetrabutyl titanate (TBOT), formic acetic acid, and ethanol are purchased from Shanghai Chemical Corp. Barium hydroxide octahydrate ($Ba(OH)_2{\cdot}8H_2O$) are purchased from Aladin. All chemicals are used without further purification. Deionized water obtained from Milli-Q system (Millipore, Bedford, MA) was used in all experiments.

2.2. Synthesis of Ultrathin $BaTiO_3$ nanowires. In a typical process, PEG-6000 (1g) was dissolved into 14 mL of ethanol. A solution of 10 mL ethanol containing 1 mmol TBOT was then added with fast stirring. After that, KOH alkaline solution (12 mL, 2M) of ethanol and deionized water were added. The mixture was stirred vigorously for 30 min and then transferred into a Teflon-lined stainless-steel autoclave with a capacity of 50 mL. Then, 0.315g (1 mmol) of $Ba(OH)_2{\cdot}8H_2O$ was added. The autoclave was heated at 200 °C for 12 h, which was subsequently cooled to room temperature. The products were centrifuged and rinsed with formic acid (0.1 M), ethanol, and deionized water several times, and dried at 60 °C for 12 h in vacuum.

2.3. Characterization. The size and morphology of the oxide products were characterized by a field-emission scanning microscope (Hitachi-4800) operated at a low working voltage of 1.0 kV to avoid of charging effect. The electron diffraction, EELS and microstructure observation were carried out using a transmission electron microscope (JEM-2100F) equipped with a postcolumn Gatan-imaging-filter (GIF-Tridium, 863) system operated at 200 kV. Powder X-ray diffraction (XRD) measurements were carried out using a Bruker D8 X-ray diffractometer (Germany) with Ni-filtere Cu KR radiation (40 kV, 40 mA). Microwave absorption properties were examined by dispersing the as-synthesized ultrathin $BaTiO_3$ nanowires into epoxy resin with a weight ratio of 1:5. A portion of the composite was coated on an aluminum substrate (180 mm × 180 mm) with a thickness of several milimeters (2−5 mm) to measure the reflection loss of the samples. The remained sample was molded into the hollow pipe of a rectangular waveguide cavity with dimensions of 10.2 mm × 2.9 mm × 1.2 mm for complex permittivity and permeability measurements at 8−18 GHz and molded into a coaxial waveguide with a size of 3 mm (inside) × 7 mm (outside) × 3 mm (height) for measurements at 2−8 GHz to ensure the data consistency. The complex relative permittivity, permeability, and reflection loss were measured with a HP8510C vector network analyzer in the 2−18 GHz range. According to the transmission line theory, the reflection loss (RL) values of different composites at a given frequency and thickness layer can be defined with the following equations

$$RL\ (\mathrm{dB}) = -20\log_{10}|(Z_{in} - 1)/(Z_{in} + 1)|$$

$$Z_{in} = \sqrt{\mu_r/\varepsilon_r}\tanh[-j(2\pi fd/c)\sqrt{\mu_r\varepsilon_r}]$$

where ε_r and μ_r are the relative complex permittivity and permeability of the absorber medium, c is the velocity of light, f is the frequency of microwave in free space, d is the coating thickness, and Z_{in} is the input impedance of the absorber. The coaxis ring, waveguide cavity, and reflection loss sheets used for microwave absorption measurements were shown in Figure S1 in the Supporting Information. And Figure S2 in the Supporting Information shows a cross-section image of the composite film, from which we can see that the powder of the ultrathin BaTiO3 nanowire is dipersing in the epoxy resin uniformly.

3. RESULTS AND DISCUSSION

Figure 1a and 1b are a low-magnification SEM image and a middle-magnification TEM image of the as-prepared sample, respectively, revealing the large quantity of nanowire materials with narrow size distribution, uniform geometrical morphology and high synthesis yield (insets of Figure 1a, b). Several tens of grams of nanowires can be simply obtained through several

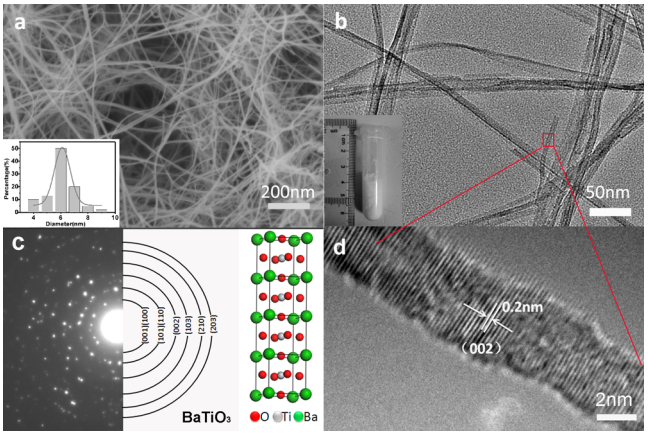

Figure 1. (a) SEM and (b) TEM images of the ultrathin $BaTiO_3$ nanowires. Inset of a is the diameter distribution histograms of the $BaTiO_3$ nanowires. Inset of b is a digital photo of the sample, showing the large quantity yield. (c) SAED pattern taken from an area containing a large amount of nanowires and (d) HRTEM image of one nanowire.

times of repeating the same synthesis (see Figure S3 in the Supporting Information).

On the basis of our careful TEM and SEM examinations, the diameters of more than 50% of the nanowires are ~6 nm. After careful statistically counting, the lengths of more than 95% of our nanowires are about several tens of micrometers. The aspect ratio is calculated as length divided by diameter of each nanowire to be more than 1300 in our case. Hence, the aspect ratio of the achieved nanowires is ultra high. A typical selected area electron diffraction (SAED) pattern taken from an area containing a large amount of nanowires is shown in Figure 1c. This SAED pattern can be well indexed to be a cubic $BaTiO_3$ phase, with the inner rings corresponding to the (100), (110), (200), (210), (211), and (220) crystalline planes. EELS data acquired from one single nanowire confirms that only Ba-$M_{4,5}$, Ti-$L_{2,3}$, and O−K edges can be found, without other impurity elements (see Figure S4 in the Supporting Information). Figure 1d is a high-resolution TEM image of one nanowire along nanowire axis direction. The lattice fringe corresponds to ~0.2 nm, which may be attributed to the (200) crystal planes of tetragonal $BaTiO_3$. The growth orientation of this nanowire is along [001] zone axis of tetragonal $BaTiO_3$.

Figure 2a shows an experimental XRD pattern obtained from the typical as-prepared products. All diffraction peaks in this pattern can be indexed quite well by a tetragonal $BaTiO_3$ cell with lattice parameters of a = 3.99 Å, c = 4.04 Å and a space group of *P4mm*, without any impurity phase. Figure 2b is a theoretical XRD simulation pattern using the $BaTiO_3$ atomic model (JCPDS No.: 05−2626) and the reflection computer code implemented in Cerius[2] software. Both experimental and calculated XRD profiles are in good agreement, confirming that our products contain tetragonal $BaTiO_3$. To accurately identify the tetragonal $BaTiO_3$ phase, symmetry breaking from cubic to tetragonal and its corresponding diffraction peak splitting were carefully considered, because the cubic $BaTiO_3$ structures have only one single diffraction peak at $2\theta \approx 45°$. Around the diffraction angle of $2\theta \approx 45°$ region (Figure 2a), an asymmetric broadening was found and can be attributed to be (200)/(002) reflections of tetragonal phase, indicating the existence of a tetragonal structure. To better characterize the crystal structure of the nws, of the tetragonal structure as obtained according to Rietveld refinement of the XRD data, we calculated the lattice parameters a, b = 3.997 and c = 4.016. So the c/a ratio of the as prepared sample is 1.004, less than the standard value of tetragonal phase $BaTiO_3$ (1.011 from JCPDS card: 05−626). Figure 2c shows the Raman spectra measured from the as-synthesized $BaTiO_3$ nanowires. Raman-active phonon modes of $BaTiO_3$ can be identified from our as-prepared sample: A1(LO) at 184 cm^{-1}, [B1, E(TO + LO)] at 308 cm^{-1}, [A1(TO), E(TO)] at 512 cm^{-1}, and [A1(LO), E(LO)] at 713 cm^{-1}. A weak peak at 250 cm^{-1} contributed from [A1(TO), E(LO)] mode of $BaTiO_3$ is observed from the Raman spectrum of the sample. The tetragonal phase of $BaTiO_3$ can be identified by the characteristic Raman peaks at 308 [B1, E(TO + LO)] and 720 cm^{-1} [A1(LO), E(LO)]. The Raman spectra of sample have Raman peaks at 308 cm^{-1} and 713 cm^{-1}, indicating that the as-synthesized nanocrystals are tetragonal $BaTiO_3$ phase. On the basis of the above TEM, XRD, EELS, and Raman spectrum analysis, it can be concluded that tetragonal $BaTiO_3$ with high purity, high synthesis yield, and high crystallinity was successfully achieved.

Next, the growth mechanism of the ultrathin $BaTiO_3$ nanowire was studied. The as-synthesized products separated

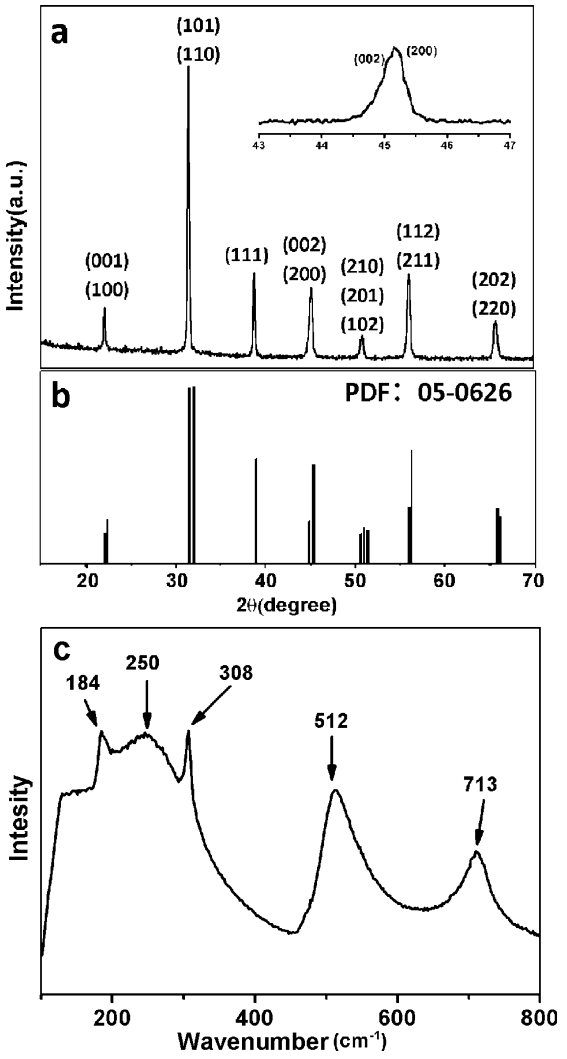

Figure 2. (a) XRD pattern of the as-prepared tetragonal $BaTiO_3$ nanowires. (b) Simulated XRD pattern of $BaTiO_3$. (c) The spectrum of the as-prepared sample.

at different reaction times (0, 0.5, 1, 4 h) are investigated respectively. Figure S5 in the Supporting Information shows the SEM images of the samples. We could see that the Ostwald ripening process is an important step in the growth of the $BaTiO_3$ nanowires. Meanwhile, PEG molecules have specific surface adsorption (interaction effect) onto the selective crystallographic planes of oxide crystals and this specific adsorption can hinder or stop the nanoparticle growth along these specific crystallographic planes, facilitating the continuous growth along other crystallographic orientations.[20] The growth of $BaTiO_3$ nanocrystals through the exposed crystallographic planes can lead to 1D nanostructures. It should be noted that when $Ba(OH)_2{\cdot}8H_2O$ was not added, the as-prepared product still keeps nanowire-like morphology (see Figure S6a in the Supporting Information). All of the diffraction peaks of the XRD pattern in Figure S6b in the Supporting Information can be indexed to a pure monoclinic phase of potassium titanate (KTO) $K_2Ti_8O_{17}$ (JCPDS No.: 84−2057). This result is similar to the previous works.[21−23] According to the results of our experiments, the strategy for synthesizing the ultrathin $BaTiO_3$ nanowires is depicted in Scheme 1. The hydrolysis of TBOT formed titanium oligomers. During the hydrothermal process, the titanium oligomers formed the nucleus of potassium

Scheme 1. Schematic Diagram of Cation Exchange Reaction and Ostwald Ripening Mechanisms for Ultrathin $BaTiO_3$ Nanowires

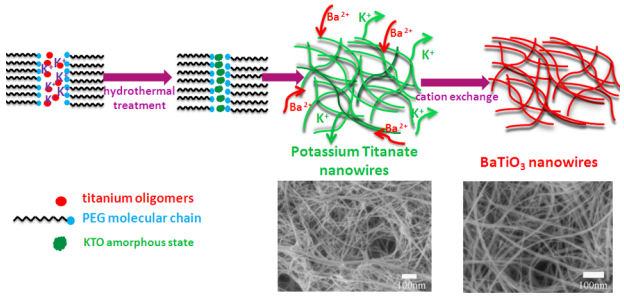

titanate (KTO) nanowires under KOH alkaline treatment according to the Ostwald ripening process. Meanwhile, the Ba^{2+} ions species in the solution can exchange with K^+ ions during the hydrothermal process. The reaction can be described as a cation exchange process. From the thermodynamics energy point of view, the propagation of the cation exchange reaction was expected to occur along the entire KTO nanowire according to the minimum principle of Gibbs free energy. Therefore, KTO was transformed to $BaTiO_3$ with the hydrothermal treatment going on, and finally $BaTiO_3$ crystalline nanowires were formed based on the Ostwald ripening process. Therefore, we propose that the synergistic effects of Ostwald ripening and the cation exchange reaction mechanisms are responsible for the growth of the ultra long $BaTiO_3$ nanowire.

Microwave absorption properties were investigated according to the methods described in the Experimental Section. Figure 3a shows the frequency dependency of the complex permittivity real part ε', permittivity imaginary part ε'', permeability real part μ', and permeability imaginary part μ'' of the $BaTiO_3$ nanowires/EP composite. The real part μ' and imaginary part μ'' for both samples nearly remain constant with frequency, indicating that $BaTiO_3$ could hardly produce any magnetic loss.

On the basis of the previous work of our group,[1] it is already known that $BaTiO_3$ nanotorus (see Figure S7a in the Supporting Information) can become promising microwave absorber. Therefore, the differences of the microwave absorption properties between the ultrathin $BaTiO_3$ nanowires and $BaTiO_3$ nanotorus are systemically compared.

The real parts (ε') of complex permittivity represents the storage capability of electric energy inside one certain type of material. The lower real part value of complex permittivity is a great advantage to strike a balance between permeability and permittivity, thus decreasing the reflection coefficient of the absorber. The ε' values of $BaTiO_3$ nanowires/EP composite decline from 8.2 to 6.7 with the measured frequency increasing from 2 to 18 GHz.

However, with the frequency increasing, the ε'' values show a different variation. The maginary parts (ε'') of complex permittivity symbolize the energy loss that caused by the electric dipole moment rearrangement under the action of electric field. As a microwave absorber, barium titanate is expected to have big imaginary parts of complex permittivity, especially in the higher frequency range. For the $BaTiO_3$ nanowires/EP composite, with the frequency increasing from 2 to 14.6 GHz, the ε'' values change upward. Between 14.6–18 GHz, the ε'' value shows a downward trend.

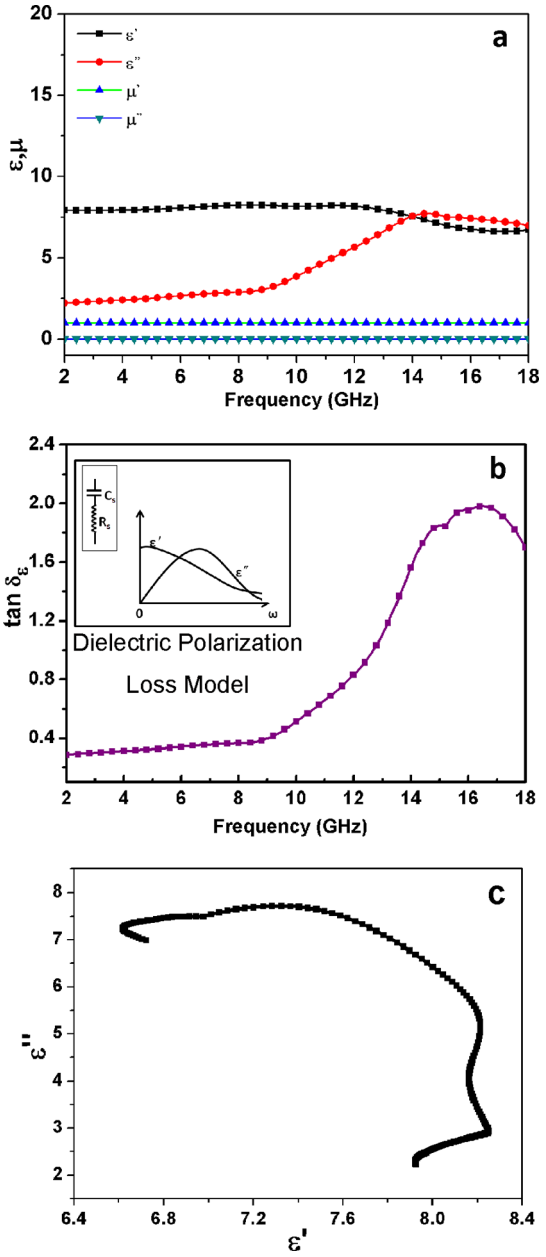

Figure 3. Frequency dependence of (a) Complex relative permittivity and permeability and (b) the dielectric loss tangent of the $BaTiO_3$ nanowires/EP composite. (c) typical Cole–Cole semicircles for $BaTiO_3$ nanowires/EP composite.

For dielectric material $BaTiO_3$, there are three factors contributing to the microwave absorption mechanisms: the dominant dielectric polarization, spontaneous polarization, and the associated relaxation effects. Different from the $BaTiO_3$ nanotorus, the real part ε' and imaginary part ε'' of $BaTiO_3$ nanowires/EP composite show the distinct similar feature of microwave absorption resulted from dielectric polarization loss (inset of Figure 3b). Hence, it is speculated that the polarization losses are the main reason of the microwave losses in ultrathin $BaTiO_3$ nanowires.

For measurement of the materials, the largerer of the electromagnetic loss angle tangent, the greater the electromagnetic wave energy is converted into other forms of energy (mainly thermal energy). The tangent values of dielectric loss ($\tan \delta_\varepsilon = \varepsilon''/\varepsilon'$) of the $BaTiO_3$ nanowires/EP composite and

dx.doi.org/10.1021/am4014506 | ACS Appl. Mater. Interfaces 2013, 5, 7146–7151

the $BaTiO_3$ nanotorus/EP composite were calculated (Figure 3b). With the frequency increasing, the tan δ_ε of the $BaTiO_3$ nanowires/EP composite increases from 0.28 to 1.98 in 2−16.5 GHz and then decline to 1.7 with the frequency ranging from 16.5 to 18 GHz. With the frequency increasing from 2−16.5 GHz, the values of dielectric loss tangent (tan $\delta_\varepsilon = \varepsilon''/\varepsilon'$) of the $BaTiO_3$ nanotorus/EP composite (see Figure S7c in the Supporting Information) gradually declines from 0.63 to 0.27.

It is interesting that the ε'' values of the $BaTiO_3$ nanowires/EP composite are larger than the ε' values in the range of 12.8−18 GHz, leading to parts of values of the tangent loss are more than 1.0.[24] It implies that the ultrathin $BaTiO_3$ nanowire is a kind of material with strong dielectric loss.

The Debye dipolar relaxation of dielectric oxide can be expressed as:\

$$(\varepsilon' - \varepsilon_\infty)^2 + (\varepsilon'')^2 = (\varepsilon_s - \varepsilon_\infty)^2$$

where ε_s and ε_∞ are stationary dielectric constant and optical dielectric constant, respectively.[20] Theoretically, the plot of ε' versus ε'' should be a single semicircle, which is usually defined as the Cole−Cole semicircle. Figure 3c shows the $\varepsilon'-\varepsilon''$ curve of the $BaTiO_3$ nanowires/EP composite over the 2−18 GHz frequency range. It can be clearly seen that there are no conspicuous semicircles in the curve. Therefore, two possible mechanisms responsible for microwave absorption are supposed: (1) there is no Debye dipolar relaxation inside of our ultrathin $BaTiO_3$ nanowires; (2) besides the loss effect resulted from Debye dipolar relaxation, there must be other absorption mechanism accounted for the ultrathin $BaTiO_3$ nanowires, both mechanisms contribute to the total microwave absorption, which deviates a standard Cole−Cole semicircle of the ε' versus ε'' plot.

Because of the isotropic crystal symmetry, isotropic antennas and some discontinuous networks in the composites will enhance the permeate of the microwave into the numerous conductive stings, which means the energy will be induced into dissipative current by random distributed isotropic antennas, resulting in the energy attenuation. The strong absorption of the ultrathin $BaTiO_3$ nanowires could be interpreted by isotropic antenna mechanism.[25] Moreover, because the aspect ratio of our nanowire is quite high (>1300), each nanowire can be considered as a microwave dissipation path, resulting into a greater impedance mismatch at air to material interface.

To reveal further the microwave absorption properties of the ultrathin $BaTiO_3$ nanowire, the reflection loss (RL) was calculated according to the transmission line theory (see Figure 4). The ultrathin $BaTiO_3$ nanowires/EP composites with the film thickness of 3.0 mm shows a maximum reflection loss of −24.56 dB at 9.04 GHz, while that of the $BaTiO_3$ nanotorus/EP composite shows −20.68 dB at 7.2 GHz with the same thickness (see Figure S7d in the Supporting Information). The frequency band lower than −10 dB of ultrathin $BaTiO_3$ nanowires/EP composites is up to 2.4 GHz (from 8 to 10.4 GHz), whereas that of nanotorus/EP composite is only 1.84 GHz (from 6.4 to 8.24 GHz). It is clear that the values of maximum reflection loss display larger and the frequency band lower than −10 dB gets broader. The shift in RL peak confirms that the location of effective absorption band can be conveniently tailored by the control of the $BaTiO_3$ nanostructures to satisfy the microwave absorption requirement for various situations.

Meanwhile, analyzed from the microwave absorption data of $BaTiO_3$ nanoparticles,[1] it is reasonable to conclude that

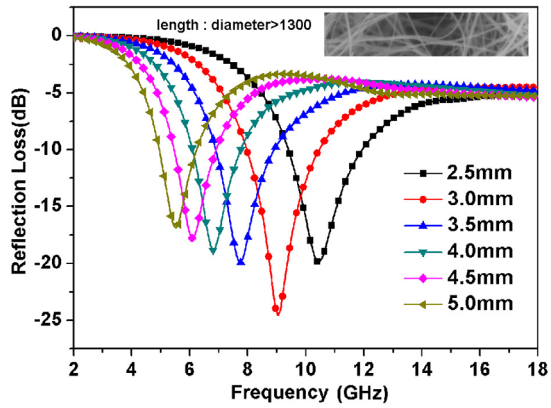

Figure 4. The reflection loss of $BaTiO_3$ nanowires/EP composite with different thicknesses.

morphology types (wire, torus, particle) can remarkably affect the microwave absorption properties of $BaTiO_3$ nanostructures.

The relatively high values of imaginary part ε'' in the range of 9.28−18 GHz is relatively higher, imply that the $BaTiO_3$ nanowires/EP composites exhibit intense dielectric losses, and the dielectric loss properties arising from the morphology variation.

Briefly, as shown in Scheme 2, there are three dominant factors contributing to the microwave absorption mechanism

Scheme 2. Schematic diagram for the microwave absorption mechanism of the ultrathin $BaTiO_3$ nanowires

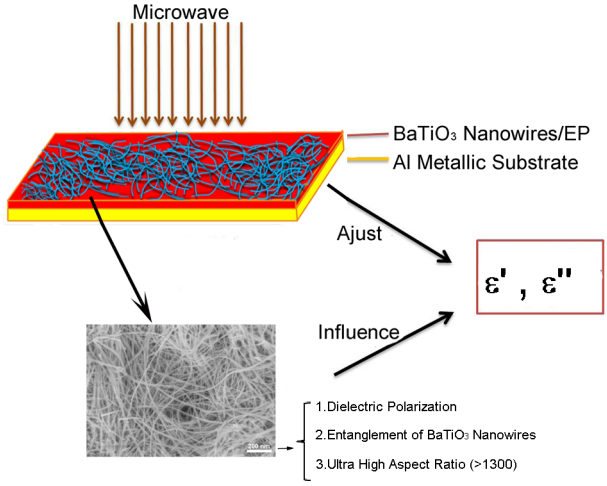

inside the dielectric ultrathin $BaTiO_3$ nanowires: (1) the inherent dielectric polarization resulted from $BaTiO_3$, (2) spontaneous polarization coupling among the entanglement/assemble of ultrathin nanowires, (3) relaxation channel with enough length (approxiately several tens of micrometers) inside ultrathin nanowires.

4. CONCLUSION

In summary, ultrathin tetragonal $BaTiO_3$ nanowires with ultra high aspect ratio (>1300) can be synthesized by a simple one-step hydrothermal method. Each nanowire has a uniform diameter of ∼6 nm and a length up to several tens of micrometers. The synergistic effects including both Ostwald ripening and cation exchange reaction are responsible for the growth of the ultrathin $BaTiO_3$ nanowire. The microwave

absorption capability of the ultrathin $BaTiO_3$ nanowires is much enhanced compared to that of $BaTiO_3$ nanoparticles, with a maximum reflection loss as high as −24.56 dB at 9.04 GHz and an absorption bandwidth of 2.4 GHz (<−10 dB). On the basis of the careful analysis of the electromagnetic parameters, a dielectric polarization mechanism is presented. Because of the simplicity and high productivity of this method, it is anticipated that this methodology can be expanded to the large-scale synthesis of other important 1D ferroelectric nanostructures. The strong microwave absorption property of ultrathin $BaTiO_3$ nanowires indicates that these nanowires could be used as a promising microwave-absorbing material.

■ ASSOCIATED CONTENT

Supporting Information

Digital photos of high yield of ultrathin $BaTiO_3$ nanowires and microwave absorption measurements equipments are provided in Figure S1−S4. EELS acquired from one single BTO nanowire is shown in Figure S5. The FESEM image and XRD pattern of potassium titanate nanowires are provided in Figures S6. The microwave absorption properties and scheme of $BaTiO_3$ nanostructures are provided in Figures S7 and S8. This material is available free of charge via the Internet at http://pubs.acs.org/.

■ AUTHOR INFORMATION

Corresponding Author

*E-mail: rcche@fudan.edu.cn. Tel: + 86 21 5163 0213.

Author Contributions

§Authors J.Y. and J.Z. contributed equally to this work.

Notes

The authors declare no competing financial interest.

■ ACKNOWLEDGMENTS

This work was supported by the National Natural Foundation of China (51172047, 50872145, and 51102050), the Ministry of Science and Technology of China (973 Project 2013CB932901 and 2009CB930803), and the This project was sponsored by Shanghai Pujiang Program and "Shu Guang" project of Shanghai Municipal Education Commission and Shanghai Education Development Foundation (09SG01).

■ REFERENCES

(1) Xia, F.; Liu, J. W.; Gu, D.; Zhao, P. F.; Zhang, J.; Che, R. C. *Nanoscale* **2011**, *3*, 3860.
(2) Zhao, H. T.; Han, X. J.; Zhang, L. F.; Wang, G. Y.; Wang, C.; Li, X. A.; Xu, P. *Radiat. Phys. Chem.* **2011**, *80*, 390.
(3) Xing, X.; Deng, J.; Chen, J.; Liu, G. *J. Alloys Compd.* **2004**, *384*, 312.
(4) Dutta, P. K.; Asiaie, R.; Akbar, S. A.; Zhug, W. D. *Chem. Mater.* **1994**, *6*, 1542.
(5) McNeal, M. P.; Jang, S. J.; Newnham, R. E. *J. Appl. Phys.* **1998**, *83*, 3288.
(6) Feteira, A.; Sinclair, D. C.; Reaney, I. M.; Somiya, Y.; Lanagan, M. T. *J. Am. Ceram. Soc.* **2004**, *87*, 1082.
(7) Liu, Y.; Feng, Y.; Wu, X.; Han, X. *J. Alloys Compd.* **2009**, *472*, 441.
(8) Fu, H.; Bellaiche, L. *Phys. Rev. Lett.* **2003**, 91.
(9) Chen, X. D.; Wang, G. Q.; Duan, Y. P.; Liu, S. H. *J. Phys. D: Appl. Phys.* **2007**, *40*, 1827.
(10) Handoko, A. D.; Goh, G. K. L. *Scie. Adv.Mater* . **2010**, *2*, 16.
(11) Urban, J. J.; Yun, W. S.; Gu, Q.; Park, H.K.. *J. Am. Chem. Soc.* **2002**, *124*, 1186.
(12) Urban, J. J.; Spanier, J. E.; Lian, O. Y.; Yun, W. S.; Park, H. K. *Adv. Mater.* **2003**, *15*, 423.
(13) Joshi, U. A.; Lee, J. S. *Small.* **2005**, *1*, 1172.
(14) Kang, S. O.; B. H., P.; Kim, Y. *Crys. Growth Des.* **2008**, *8*, 3180.
(15) Kang, S. O.; Jang, H. S.; Kim, K. B.; Park, B. H.; Jung, M. J.; Kim, Y. I. *Mater. Res. Bull.*. **2008**, *43*, 996.
(16) Mao, Y. B.; B., S.; Wong, S. S. *J. Am. Chem. Soc.* **2003**, *125*, 15718.
(17) Huang, K. C.; Huang, T. C.; Hsieh, W. F. *Inorg. Chem.* **2009**, *48*, 9180.
(18) Zhu, Y. F.; Zhang, L.; Natsuki, T.; Fu, Y. Q.; Ni, Q. Q. *ACS App. Mater. Interfaces* **2012**, *4*, 2101.
(19) Zhu, Y. F.; Fu, Y. Q.; Natsuki, T.; Ni, Q. Q. *Polym. Compos.* **2013**, *34*, 265.
(20) Karakoti, A. S.; Das, S.; Thevuthasan, S.; Seal, S. *Angew. Chem.* **2011**, *50*, 1980.
(21) Du, G. H.; Chen, Q. P.; Han, D.; Yu, Y.; Peng, L. M. *Phy. Rev. B* **2003**, *67*.
(22) Xu, J.; Zhang, H.; Li, W.; Zhang, J.; Liu, X.; He, X.; Xu, D.; Qian, J.; Liu, L. *Micro. Nano Lett.* **2012**, *7*, 654.
(23) Yuan, Z. Y.; Zhang, X. B.; Su, B. L. *Appl. Phys. A: Mater. Sci. Proc.* **2004**, *78*, 1063.
(24) Guerra, J. de Los S.; Lente, M. H.; Eiras, J. A. *Appl. Phys. Lett.* **2006**, *88*, 102905.
(25) Zhuo, R. F.; Qiao, L.; Feng, H. T.; Chen, J. T.; Yan, D.; Wu, Z. G.; Yan, P. X. *J. Appl. Phys.* **2008**, *104*, 094101.